Selective imaging of microplastic and organic particles in flow by multimodal coherent anti-Stokes Raman scattering and two-photon excited autofluorescence analysis

Tomoko Takahashi,[*,†,‡,¶] Krzysztof Herdzik,[‡] Konstantinos Bourdakos,[‡] James Read,[‡] and Sumeet Mahajan[*,‡]

†*Advanced Science-Technology Research Program (ASTER), Japan Agency for Marine-Earth Science and Technology (JAMSTEC), 2-15 Natsushima-cho, Yokosuka, Kanagawa 2370061, Japan*

‡*Department of Chemistry and the Institute for Life Sciences, University of Southampton, Highfield Campus, Southampton SO17 1BJ, UK*

¶*Institute of Industrial Science, The University of Tokyo, 4-6-1, Komaba, Meguro-ku, Tokyo 1538505, Japan*

E-mail: takahas@jamstec.go.jp; s.mahajan@soton.ac.uk

Abstract

Microplastic pollution is an urgent global issue. While spectroscopic techniques have been widely used for identification of plastics collected from aquatic environments, these techniques are often labour-intensive and time-consuming due to sample collection, preparation and long measurement times. In this study, a method for two-dimensional detection and classification of flowing microplastic and organic particles with high spatial and temporal resolutions has been proposed based on simultaneous detection of

coherent anti-Stokes Raman scattering (CARS) and two-photon excited autofluorescence (TPEAF) signals. Poly(methyl methacrylate) (PMMA), polystyrene (PS), and low-density polyethylene (LDPE) particles with the size of several tens to hundreds of μm were selectively detected in flow with an average velocity of 4.17 mm/s by CARS line scanning. With the same velocity of flow, flowing PMMA and alga particles were measured using a multimodal system of CARS and TPEAF signals. The average intensity of both PMMA and alga particles in the CARS signals at the frequency of 2940 cm^{-1} were higher than the background level, while only algae emit TPEAF signals. Therefore, classification of PMMA and alga particles in flow has been successfully performed by simultaneous detection of CARS and TPEAF signals. With the proposed method, monitoring of microplastics in continuous water flow without collection or extraction is possible, which is game-changing for current sampling-based microplastic analysis.

Introduction

Hundreds of millions of tons of plastic waste are generated every year.[1] It is estimated that 150 million metric tons of plastics already exist in the ocean with millions of tons per year being added.[2] Plastic bags and pieces are often discovered from guts of dead seabirds and turtles.[3,4] The global awareness of plastic pollution of the marine environment has risen as highlighted in recent G7,[5] and the density of plastic debris in the ocean has been selected as an indicator of the Goal 14 of Sustainable Development Goals set by the United Nations for the year 2030.[6] In particular, microplastics, whose size is defined as less than 5 mm,[7] are easily attached to and ingested by organisms, and their ecological impact is subject to multiple studies.[8–11] These microplastic pieces are found not only in the sea but in any aquatic environments[12] and even in drinking water,[13] and are the threat to the ecosystems. To understand the dynamic spatial and temporal distributions of microplastics on local and global scales in short and long terms, fast and continuous monitoring of microplastics is necessary.

According to a typical protocol of microplastic measurements,[7] floating microplastic pieces are first collected together with other particles and organisms using a neuston net towed by a ship, and separated by their densities after dissolving organic matters, and collected on a filter. After drying, the plastic type of each particle is analysed most commonly by using the techniques of Fourier-transform infrared (FT-IR) and Raman spectroscopy.[14–17] While thermal analysis is also used for plastic identification, spectroscopic techniques are more widely used since these perform label-free, non-destructive analysis and can determine the shape and size by combining with microscopy.[18] FT-IR and Raman spectroscopy are often compared with each other. Typically, Raman spectroscopy has a better spatial resolution as a laser with a lower wavelength can be used as an excitation light source; detection of objects with sizes down to 100 nm is possible with Raman spectroscopy,[19] compared to 20 μm for FT-IR spectroscopy.[20] However, Raman spectra often suffer interference due to fluorescence caused by attached organic and inorganic matter, additives, and photodegradation, which is not a problem for FT-IR spectroscopy.[21] A limitation of both techniques is that long time is required for data acquisition. While target pre-selection by processing bright field images can reduce the total analysis time,[22] the long measurement time, typically several seconds per spectral acquisition, is inherent to the techniques. Shim et al. reported that measurements using FT-IR spectroscopy typically require several hours.[18] While automated chemical mapping can reduce the time for manual-intensive work and also has less operator bias,[23] the information available using current methods tends to be discrete due to the limitation of the measurement time.

Compared to FT-IR spectroscopy, Raman spectroscopy has a big advantage in analysis of submerged targets in water since visible and near infrared (NIR) laser beams, which penetrate further in water than ultraviolet (UV) and IR beams, can be used as an excitation light source. Using Raman spectroscopy, identification of types of plastic pellets in a large water volume has been successfully performed.[24] Detection of flowing microplastics with the size of more than 100 μm has also shown to be possible.[25] These studies demonstrate the feasibility

of Raman spectroscopy for screening of microplastics without extraction. Coherent anti-Stokes Raman scattering (CARS), which is applicable to micro-sized particle measurements in water, has huge potential to reduce the data-acquisition time and provide imaging capability. Compared to a weak Raman signal, whose intensity is one-ten millionth of irradiated laser power, a CARS signal is significantly strong due to vibrational coherence generated by irradiating pump and Stokes laser beams whose wavelength difference matches the frequency of the target's molecular vibration.[26] Moreover, CARS images are free from interference due to one-photon excited fluorescence unlike Raman spectroscopy. The technique has been often applied to in vivo imaging of biomedical samples, in particular live cells.[27–29] The application fields of CARS are expanding, such as imaging of marine microalegae.[30] While microplastics are an ideal target for CARS since many molecular bands of plastic structures are CARS-active, the application of CARS to microplastics has been reported only in relatively few studies. After the first report by Cole et al., where ingested and attached micro beads of polystyrene by zooplankton were detected using CARS,[31] Zada et al. demonstrated fast microplastic identification of 5 different types of microplastics fixed on a slide glass using stimulated Raman scattering (SRS), another coherent Raman technique.[32] Recent research has demonstrated detection of micro-sized standard plastic beads in flow in a microfluidic device using CARS and fluorescence line-scanning flow cytometry,[33] CARS combined with linear scattering[34] and FT-CARS spectroscopic flow cytometry.[35] Particularly, the shape of flowing particles can be reconstructed from line-scan CARS images without taking additional optical images. These techniques are often applied to cell analysis and could be potentially used for continuous chemical measurements of particles in aquatic environments to monitor microplastic pollution. However, practical microplastic-related studies aiming at continuous monitoring using these techniques are not yet reported possibly due to a strict flow control to align particles to a small measurement area in a microfluidic device.

In this study, to investigate the feasibility of CARS for continuous microplastic monitoring, we perform two-dimensional imaging of microplastics in flow in a fluidic device using

CARS. Selective imaging of plastic particles of three different polymers is performed in flow with an average velocity of 4.17 mm/s. With the same velocity, simultaneous classification of microplastics and algae using a multimodal system of CARS and two-photon excited auto fluorescence (TPEAF) analysis is further demonstrated. Using this method, plastic and organic particles flowing in a plane can be chemically classified along with their shape information. This study indicates the possibility of on-site, fully-automated microplastic measurements without sampling from aquatic environments such as oceans, rivers, and lakes.

Experimental section

Materials

The following standard plastic beads were used during in-flow measurements; poly(methyl methacrylate) (PMMA) beads with the size of 40±18 μm (Colacryl D150, Songhan Plastic Technology Co.,Ltd.), polystyrene (PS) beads with the size of 39.5±1.0 μm (Duke Standards, ThermoFisher Scientific). Irregular-shaped LDPE particles with the maximum size of 300 μm were also used for in-flow tests (ET316031, GoodFellow Cambridge Ltd.). For static measurements of plastics, since all three plastic particles were measured in the same field of view, large PS beads with the size of 200±1.0 μm (16435-5ML, Sigma-Aldrich) were instead used to recognise particle types visually. The diameter range of PMMA beads was obtained by processing binary images created from bright field images of 224 beads using ImageJ-Fiji (Version 1.52p[36]). The diameter ranges of PS beads and maximum size of LDPE particles were obtained from supplier information. The density of PMMA, PS and LDPE is 1.19, 1.05, and 0.94 g/cm^3, respectively. These plastics are typically found in aquatic environments.[12] Scenedesmus, a freshwater algae (Scenedesmus Algae - Live, Breckland Scientific) was used as an organic particle. Fig. 1 shows bright field images of (a) PS and PMMA beads, (b) LDPE particles, and (b) Scenedesmus. The algae's shape is easily distinguished from spherical plastic particles.

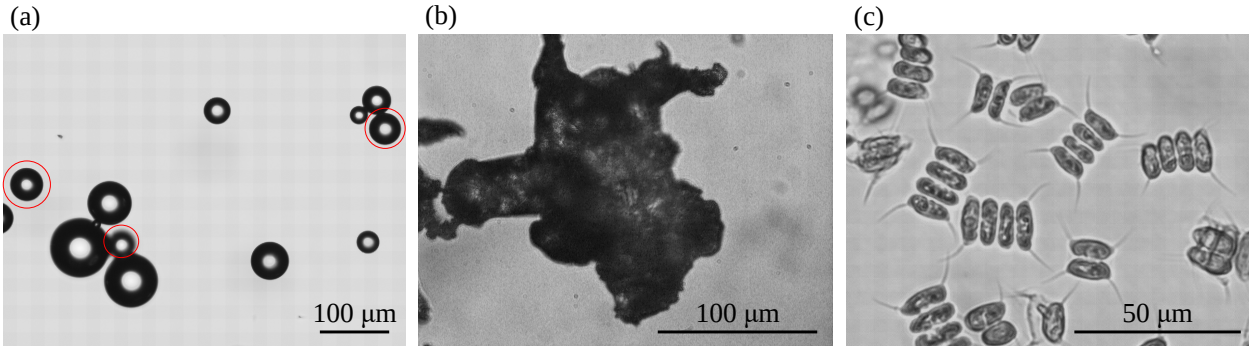

Figure 1: Bright field images of (a) PS and PMMA particles, (b) LDPE particles, and (c) Scenedesmus. The red circles in (a) indicate PS particles. The remainder in beads in (a) is PMMA particles.

Experimental setup

The experimental setup is shown in Fig. 2. A fibre laser (APE, Emerald Engine) with the wavelength of 1031 nm, pulse duration of 2 ps, and repetition rate of 80 MHz is used as a Stokes beam. A pump beam with the wavelength range from 650 to 950 nm is generated using an optical parametric oscillator (OPO) (APE, Levante Emerald) pumped by a frequency doubled beam obtained from the 1031 nm fundamental. As shown in Fig. 2, two synchronously generated beams are combined using a shortpass dichroic beam splitter (shown as SPD1) with a cutoff wavelength of 970 nm (970spxr-xxt, Chroma). The collinear beams are temporally and spatially overlayed. A shortpass dichroic beam splitter (shown as SPD2) with a cutoff wavelength of 750 nm (750spxrxt, Chroma) is used to direct the beams on to a sample through an objective lens. The generated signals are collected in an epi-detection mode through the same objective and pass through the SPD2. CARS signals are detected by a photomultiplier tube (H10722-20, Hamamatsu Photonics; shown as PMT1) through a longpass dichroic beam splitter (shown as LPD1) with a cutoff wavelength of 442 nm (DI02-R442, Semrock) for detection of only CARS signals and 594 nm (DI02-R594, Semrock) for simultaneous detection of CARS and TPEAF signals, shortpass filter (shown as SP1) with a cutoff wavelength of 775 nm (BrightLine Fluorescence Filter 775/SP, Semrock), and bandpass filter (shown as BP1) with a wavelength of 643±20 nm (BrightLine 643/20, Semrock).

TPEAF signals, reflected at LPD1, are simultaneously recorded by another photomultiplier tube (shown as PMT2) located after a bandpass filter (shown as BP2) with a wavelength of 550±40 nm (FB550-40,Thorlabs). Two-dimensional chemical imaging is done by scanning the laser beam using a galvanometric scanner. ScanImage 5.1 (Vidrio Technologies) is used for acquiring images with the laser scanning microscope.[37] The total incident power on the sample was 180 mW (120 mW from pump and 60 mW from Stokes) during in-flow measurements and static measurements of a PMMA and algae mixture, and 90 mW (60 mW from pump and 30 mW from Stokes) during static measurements of a plastic mixture, which were experimentally determined as an optimal. An objective lens with 10 × magnification and the numerical aperture (NA) of 0.30 (CFI Plan Fluor 10 ×, Nikon Instruments Inc.) was used for plastics. When algae were mixed, an objective lens with 20 × magnification and the NA of 0.50 (CFI Plan Fluor 20 ×, Nikon Instruments Inc.) was used because the average size of algae is approximately 20 μm, twice smaller than PMMA beads.

Flow device

Detection of flowing particles was performed using a quartz glass flow cell (48-Q-0.5, Starna Scientific Ltd.) with the inner thickness of 500 μm, width of 8 mm, and the length of 40 mm. Polytetrafluoroethylene (PTFE) tubes with an internal diameter of 1.5 mm were connected to inlet and outlet pipes. The inlet tube was connected to a glass syringe which was automatically pumped using a syringe pump (Fusion 100, Chemyx Inc.). The water flow rate was set to 1 ml/min, which was experimentally found to be optimal to stably detect particles. The flow rate of 1 ml/min is equivalent to the average velocity in the flow device of 4.17 mm/s. When only plastic samples were measured saturated sodium chloride solution, with a density higher than all plastics used in this work, was used as a medium to allow all particles float near the surface and to diminish an effect of buoyancy of the particles due to the relative density to a medium as this would have affected the relative signals and hence, detection in flow for comparative purposes. For classification tests of plastic beads and algae, the purified

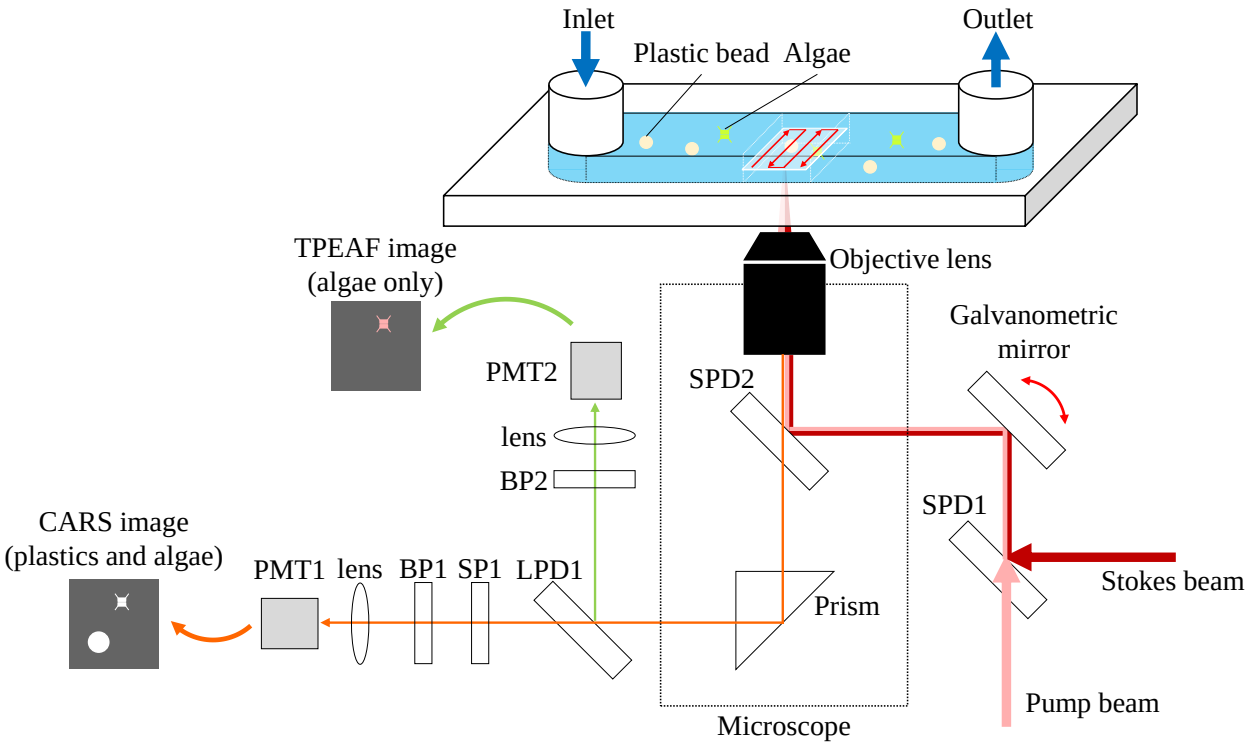

Figure 2: Experimental setup. SPD, shortpass dichroic beam splitter; LPD, longpass dichroic beam splitter; BP, bandpass filter; SP, shortpass filter; PMT, photomultiplier tube.

water was used since Scenedesmus is a freshwater green alga.

Results and discussions

CARS and TPEAF images of static samples

CARS images of dry PMMA, PS and LDPE particles are shown in Fig. 3. The large spherical particle seen in the upper part in (a) is a PS bead with the size of 200 μm, small spherical particles are PMMA beads with the size of 40 μm, and an irregular shaped particle seen in the lower part is a LDPE particle with the size of 300 μm. The same field of view shown in (a) was scanned using CARS with the detected CARS signals of (b) 2840 cm^{-1}, (c) 2940 cm^{-1}, and (d) 3050 cm^{-1}, respectively. The CARS signals at 2840, 2940 and 3050 cm^{-1} correspond to the peak attributed to the asymmetric CH stretch vibration which LDPE has as a main

structure, aliphatic CH_3 which PMMA has, and the aromatic CH stretch vibration mode which PS has, respectively.[26] In (b), (c) and (d), it can be seen that the area where LDPE, PMMA, and PS particles are seen is brightly illuminated, respectively. To quantitatively evaluate the intensity difference of CARS signals between plastic types, the average intensity from each particle at each frequency is calculated as shown in Fig. 4. The black circles and line indicate LDPE, red squares and line indicate PMMA, and blue triangles and line indicate PS. The calculation method is explained in the Supporting Information (SI). From Fig. 4, it is clearly demonstrated that plastic types are classified with the corresponding frequencies.

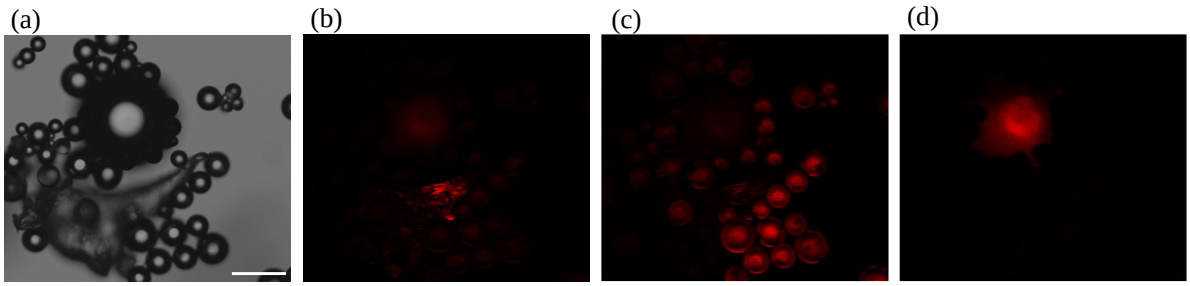

Figure 3: (a) Bright field image of PMMA, PS, and LDPE particles, and CARS images of the same field of view for (b) 2840 cm^{-1} (LDPE active), (c) 2940 cm^{-1} (PMMA active) and (d) 3050 cm^{-1} (PS active). The scale bar indicates 100 μm. The large spherical particle is a PS bead with the size of 200 μm, small particles are PMMA beads with the size of 40 μm, and an irregular shaped particle is a LDPE particle with the size of 300 μm.

For classification of plastics (PMMA) and algae, CARS and TPEAF images were taken simultaneously. The CARS signals at the frequency of 2940 cm^{-1} are shown in red, and the TPEAF signals at the wavelength between 530 and 570 nm are shown in green in Fig. 5. Since algae have CH bonds, both a PMMA bead and algae are detected in the CARS image, but the PMMA bead has higher intensity than algae. In the TPEAF image, it is clearly seen that only algae are detected because of the existence of chlorophyll.

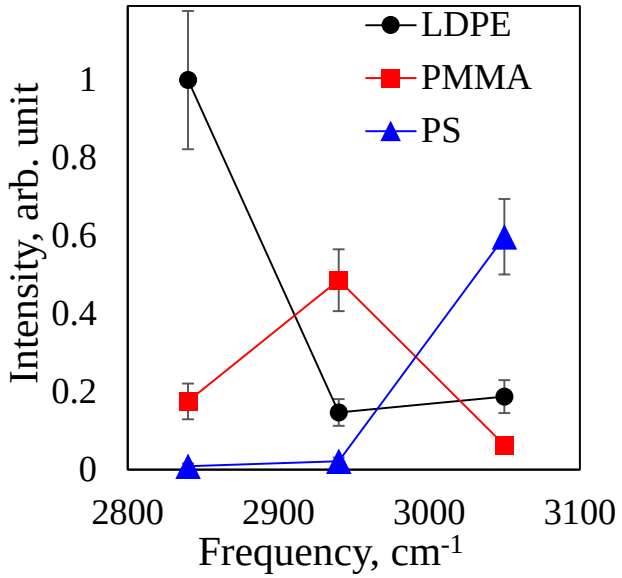

Figure 4: the average intensity of CARS signals from LDPE, PMMA, and PS particles at the frequency of 2840, 2940, and 3050 cm^{-1}. The black circles and line indicate LDPE, red squares and line indicate PMMA, and blue triangles and line indicate PS.

Selective 2D imaging of microplastics in flow

Fig. 6 shows (a) an example of CARS images of PS beads with the size of 39.5 μm in flow with the average velocity of 4.17 mm/s and the detected frequency of 3050 cm^{-1}. (b) indicates zoomed CARS images of PS, PMMA, and LDPE particles with the detected frequency of 3050 cm^{-1}, 2940 cm^{-1}, 2840 cm^{-1}, respectively, which corresponds to detection of each type of particles. Similar to the static images shown in Fig. 3, spherical PS and PMMA particles are illuminated uniformly, while LDPE particles are illuminated unevenly due to the irregular shape and rough surface. The false negative rate was calculated for spherical particles, *i.e* PS and PMMA, for which a particle can be defined as a cluster of pixels with the intensity of higher than a threshold. The criterion of particle detection is described in detail in the Supporting Information (SI). Under the criterion, the false negative rate was zero at the frequencies of 3050 cm^{-1} for PMMA and 2940 cm^{-1} for PS. From the result, it can be said that flowing plastic particles can be clearly identified when the corresponding

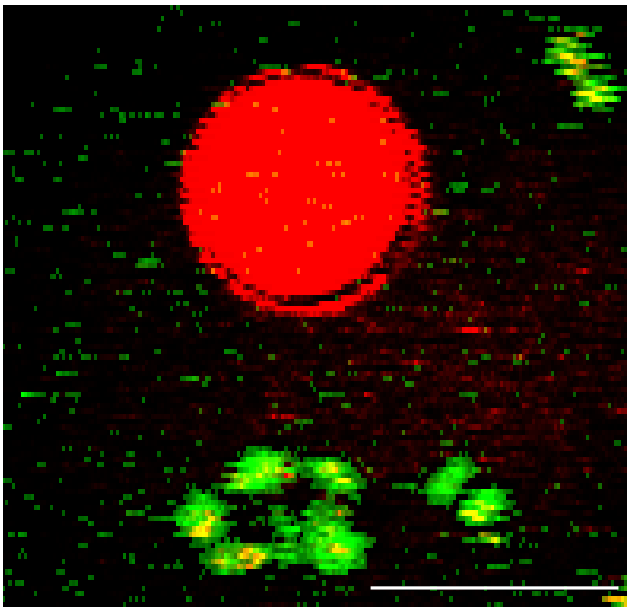

Figure 5: Superimposed image of CARS (red) and TPEAF (green) signals. A PMMA bead is detected by CARS (2940 cm^{-1}) and algae are detected by CARS and TPEAF signals. The scale bar indicates 50 μm.

CARS signals are observed. To quantitatively evaluate the accuracy of particle detection, flow tests with two different concentrations of PMMA beads were performed; (concentration 1) 1.12 weight % and (concentration 2) 2.25 weight % of PMMA beads in saturated sodium chloride solution. It should be noted that the concentration of plastic particles used in this study is higher than typical natural environments,[38] although the abundance of plastics with the size of $< 300\,\mu$m is not well known. While in this study, these concentration ranges were selected to demonstrate the reliability of detection as a proof-of-concept, this technique is applicable to any concentration range since flow with particles can be continuously measured and the proposed method can detect at the single particle level. During the measurement for 200 seconds, 143 and 343 particles were detected for the test with concentration 1 and 2, respectively, which is coherent with the concentration difference. It should be noted that the size of detected particles depends on the location of particles in depth and particle speed as particles with different widths and lengths are observed in Fig. 6, and does not always match the actual size. Although this does not affect the result of particle counting, calibration of

effects of these values is required for further morphological analysis. These can be measured using particle imaging velocimetric methods,[39,40] which will be investigated in further studies. A method for reliable detection and counting of irregular-shaped particles is necessary for the application to aquatic environments, and image processing methods possibly based on machine learning are promising to reconstruct the shape of sparsely illuminated targets.[41] In this study, different plastic types are separately investigated in each flow due to the technical limitation of the setup which requires ~ 1 minute to modulate the wavelength of the pump beam. This will be overcome with a setup with either multiple wavelengths or ultrafast wavelength modulation capability or a flow-cell path long enough to change the wavelength to another, as well as other CARS-based methods, *e.g.* FT-CARS, with which a CARS spectrum can be obtained with the speed of $370\,\mu$s/point.[35] It should be also noted that only particles in focus and within the field of view are sampled by the proposed method. It can be still a powerful tool for monitoring of particles by obtaining representative data of randomly selected particles from a number of flowing particles. While a channel with the depth of similar to particle sizes is one solution to increase the number of detected particles, it might lead to clogging of the device when different sizes of particles are mixed in flow, which is expected during monitoring of particles in aquatic environments. Alternatively, three dimensional line scanning, *i.e*, z direction scanning along with current x-y direction scanning is possible and this enables scanning of a flow channel with a relatively large depth compared to microfluidic devices.

Simultaneous classification of plastics and algae

Fig. 7 indicates particle images of CARS signals ($2940\,\mathrm{cm}^{-1}$) shown in red and TPEAF signals shown in green in continuous flow of mixed PMMA and alga particles with the average velocity of $4.17\,$mm/s. The image sets shown in (a) and (b) are PMMA beads and algae, respectively, which are determined from their size and shape in CARS images. While both types of particles are clearly detected in CARS images, only algae are detected in TPEAF

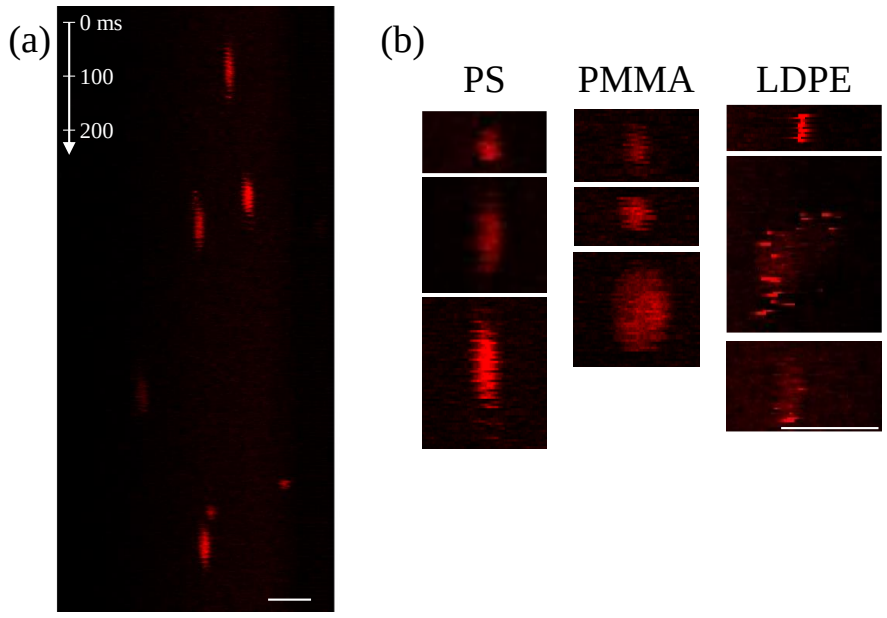

Figure 6: (a) Example of CARS images of PS beads with the size of 39.5 μm in flow with the average velocity of 4.17 mm/s and the detected frequency of 3050 cm^{-1}. The scan speed and direction are indicated in (a). (b) Zoomed CARS images of PS, PMMA, and LDPE particles with the detected frequency of 3050 cm^{-1}, 2940 cm^{-1}, 2840 cm^{-1}, respectively. The scale bars indicate 100 μm.

signals. The CARS signal intensity of pixels within a detected particle was averaged for both static and flowing particles, and the average intensity of each particle type and condition is shown in Table 1. "Number" indicates the number of particles. The intensity of each particle is shown in Table S1. The CARS intensity is on average 0.93 (static) and 0.95 (flow) for plastics and 0.76 (static) and 0.77 (flow) for algae. All particles detected during both static and flow measurements have higher CARS signal intensities than the background level, which is 0.14 for static measurements and 0.24 for measurements in flow, while the intensities of plastics are slightly higher than algae. A difference between plastics and algae is seen in the TPEAF signal intensity. While the TPEAF signal intensity of plastics, which is on average 0.038 (static) and 0.060 (flow), is similar to the background intensity of 0.042 (static) and 0.055 (flow), all alga particles have twice to 5 times higher intensity than the background. This result provides the proof-of-concept of simultaneous classification of plastic ad organic particles using a multimodal CARS and TPEAF system. With two-dimensional scanning of

flowing particles, shape information is also available without an extra image capturing system such as a high-speed camera. It should be noted that in the current method if a certain type of plastics emits in the range of 550±40 nm then using the TPEAF signals will not be able to distinguish them from algae. However, in CARS the excitation wavelengths can be tuned yet the same vibrational frequencies can be targeted, and also in the multimodal detection system different or multiple emission wavelengths can be collected to suit distinction. While further studies will be necessary to investigate classification ability of this method by intensity difference of natural organic particles and plastics which emit in the same wavelength range, it is not a fundamental limitation of the method we have described in this work, and the proposed method can still be a powerful tool to classify most microplastics and natural organic matter. The technique is applicable to drinking water quality control to monitor microplastic contamination, where microplastics with the size of several to several tens of μm are often found.[20] Continuous monitoring of microplastics in flow in aquatic environments will be also possible without separation and extraction from other organic particles. For applications to aquatic environments, it should be noted that biofilms formed on the surface of plastics[42] could interfere with the detection of signals and future studies are required to investigate difference of the signal intensity of biofilm coated particles and pure organic materials. However, considering that CARS uses NIR light which penetrates deeper into material than UV and VIS light due to reduced scattering and signals are free from one-photon excited fluorescence, CARS and TPEAF signals from particle materials can be collected. It has been reported that biofilm thickness was experimentally found to be about 30 μm after immersion in seawater for more than hundred days,[43] and this is within the penetration depth of NIR light through biofilms, which is typically $> 50\,\mu$m.[44,45] As we demonstrated in this study, since TPEAF and CARS signals can be simultaneously and separately collected, TPEAF signals from biofilms are likely to provide complementary information rather than overwhelm the CARS signal or diminish detection ability. To perform in-depth analysis of a flowing particle, three-dimensional line scanning, which is discussed in the previous section,

will be of help, and investigated in future studies. In addition, device development aiming at a robust measurement system without clogging of a fluidic device, *e.g.* installing size separation mechanism,[46] is necessary for future field tests where particles with various shapes and sizes are expected. The proposed method will enable collecting dynamic information of microplastic distributions in significantly high spatial and temporal resolutions, which is not possible to realise with methods currently available. Abundance of both organic matter and plastics can be obtained using this method, which is important to assess environmental impacts of plastics on biomass and biodiversity.[47] Continuous monitoring will contribute to understanding of changes of microplastics daily or even every second at a certain location and this will help monitor and control the water quality. In addition, by continuous monitoring using this method on a ship or automated surface vehicles, spatial resolution or localisation of the data will be significantly improved compared to sampling-based methods.

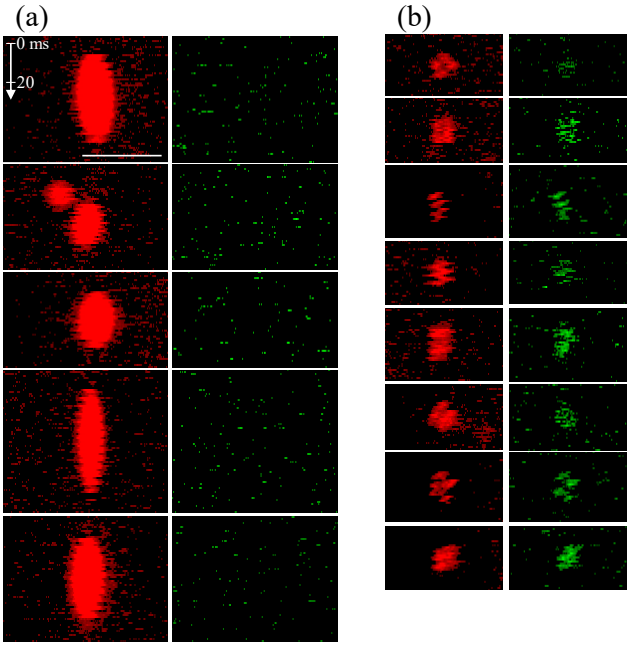

Figure 7: (Left) CARS signals ($2940\,\mathrm{cm}^{-1}$) shown in red and (right) TPEAF signals shown in green for (a) PMMA particles and (b) alga particles in continuous flow with the average velocity of $4.17\,\mathrm{mm/s}$. The scale bar indicates $50\,\mu\mathrm{m}$. The scan speed and direction are indicated in (a).

Table 1: Average intensity of CARS and TPEAF signals for static and flowing particles. "Number" indicates the number of particles.

	Number	**CARS**	**TPEAF**
Background (static)	-	0.14 ± 0.19	0.042 ± 0.028
PMMA	2	0.93 ± 0.01	0.038 ± 0.010
Alga	3	0.76 ± 0.04	0.16 ± 0.04
Background (flow)	-	0.24 ± 0.11	0.055 ± 0.027
PMMA	6	0.95 ± 0.03	0.060 ± 0.004
Alga	8	0.77 ± 0.04	0.11 ± 0.02

Conclusions

This study has demonstrated identification of microplastic beads and organic particles in flow by two-dimensional simultaneous CARS and TPEAF imaging. PMMA and PS beads with the size of 40 μm and LDPE particles with the maximum size of 300 μm were selectively detected in flow with an average velocity of 4.17 mm/s by CARS imaging. The multimodal system of CARS and TPEAF signal detection further demonstrated simultaneous classification of plastic and organic particles in flow with the same velocity. The proposed method will enable microplastic classification in continuous flow with a large volume without separation nor preparation, and will lead to a better understanding of dynamics of microplastic distributions in high spatial and temporal resolutions.

Acknowledgement

This work was supported by Kajima Foundation (Overseas research grant), JSPS KAKENHI Grant (18K13934), Kurita Water and Environment Foundation (17B030), and the European Research Council (ERC) grant NanoChemBioVision (638258).

Supporting Information Available

The following files are available free of charge.

- Details on methods for particle detection including:
  - Table S1: Average intensity of at each particle region at each frequency with the standard deviation and Figure
  - Figure S1: Cropped regions in the bright field image of PMMA, PS, LDPE particles and background.
- Details on CARS and TPEAF signals including:
  - Intensity of CARS and TPEAF signals for static and flowing particles of PMMA and algae.

References

(1) Jambeck, J. R.; Geyer, R.; Wilcox, C.; Siegler, T. R.; Perryman, M.; Andrady, A.; Narayan, R.; Law, K. L. Plastic waste inputs from land into the ocean. *Science* **2015**, *347*, 768–771.

(2) Ocean Conservancy and McKinsey Center for Business and Environment, *Stemming the Tide: Land-based strategies for a plastic-free ocean*; 2015.

(3) Moore, C. J. Synthetic polymers in the marine environment: A rapidly increasing, long-term threat. *Environmental Research* **2008**, *108*, 131–139.

(4) Cole, M.; Lindeque, P.; Halsband, C.; Galloway, T. S. Microplastics as contaminants in the marine environment: A review. *Marine Pollution Bulletin* **2011**, *62*, 2588–2597.

(5) Williamson, P., Smythe-Wright, D., Burkill, P., Eds. *Future of the Ocean and its Seas: A non-governmental scientific perspective on seven marine research issues of G7 interest*; 2016; ICSU-IAPSO-IUGG-SCOR.

(6) United Nations General Assembly, *Work of the Statistical Commission pertaining to the 2030 Agenda for Sustainable Development*; 2017; A/RES/71/313.

(7) Masura, J.; Baker, J. E.; Foster, G. D.; Arthur, C.; Herring, C. Laboratory methods for the analysis of microplastics in the marine environment: recommendations for quantifying synthetic particles in waters and sediments. **2015**, NOAA Technical Memorandum NOS-OR&R-48.

(8) Wright, S. L.; Thompson, R. C.; Galloway, T. S. The physical impacts of microplastics on marine organisms; A review. *Environmental Pollution* **2013**, *178*, 483–492.

(9) Setälä, O.; Fleming-Lehtinen, V.; Lehtiniemi, M. Ingestion and transfer of microplastics in the planktonic food web. *Environmental Pollution* **2014**, *185*, 77–83.

(10) Desforges, J. P. W.; Galbraith, M.; Ross, P. S. Ingestion of Microplastics by Zooplankton in the Northeast Pacific Ocean. *Archives of environmental contamination and toxicology* **2015**, *69*, 320–330.

(11) Neves, D.; Sobral, P.; Ferreira, J. L.; Pereira, T. Ingestion of microplastics by commercial fish off the Portuguese coast. *Marine Pollution Bulletin* **2015**, *101*, 119–126.

(12) Duis, K.; Coors, A. Microplastics in the aquatic and terrestrial environment: sources (with a specific focus on personal care products), fate and effects. *Environmental Sciences Europe* **2016**, *28*, 2.

(13) Eerkes-Medrano, D.; Leslie, H. A.; Quinn, B. Microplastics in drinking water: A review and assessment. *Current Opinion in Environmental Science & Health* **2019**, *7*, 69–75.

(14) Thompson, R. C.; Olsen, Y.; Mitchell, R. P.; Davis, A.; Rowland, S. J.; John, A. W. G.; McGonigle, D.; Russell, A. E. Lost at Sea: Where Is All the Plastic? *Science* **2004**, *304*, 838–838.

(15) Ribeiro Claro, P.; Nolasco, M.; Araújo, C. Characterization of Microplastics by Raman Spectroscopy. *Comprehensive Analytical Chemistry* **2016**, *75*, 119–151.

(16) Xu, J. L.; Thomas, K. V.; Luo, Z.; Gowen, A. A. FTIR and Raman imaging for microplastics analysis: State of the art, challenges and prospects. *TrAC - Trends in Analytical Chemistry* **2019**, *119*, 115629.

(17) Anger, P. M.; von der Esch, E.; Baumann, T.; Elsner, M.; Niessner, R.; Ivleva, N. P. Raman microspectroscopy as a tool for microplastic particle analysis. *TrAC - Trends in Analytical Chemistry* **2018**, *109*, 214–226.

(18) Shim, W. J.; Hong, S. H.; Eo, S. E. Identification methods in microplastic analysis: a review. *Anal. Methods* **2017**, *9*, 1384–1391.

(19) Sobhani, Z.; Zhang, X.; Gibson, C.; Naidu, R.; Megharaj, M.; Fang, C. Identification and visualisation of microplastics/nanoplastics by Raman imaging (i): Down to 100 nm. *Water Research* **2020**, *174*.

(20) Schymanski, D.; Goldbeck, C.; Humpf, H. U.; Fürst, P. Analysis of microplastics in water by micro-Raman spectroscopy: Release of plastic particles from different packaging into mineral water. *Water Research* **2018**, *129*, 154–162.

(21) Cabernard, L.; Roscher, L.; Lorenz, C.; Gerdts, G.; Primpke, S. Comparison of Raman and Fourier Transform Infrared Spectroscopy for the Quantification of Microplastics in the Aquatic Environment. *Environmental Science and Technology* **2018**, *52*, 13279–13288.

(22) Araujo, C. F.; Nolasco, M. M.; Ribeiro, A. M.; Ribeiro-Claro, P. J. Identification of microplastics using Raman spectroscopy: latest developments and future prospects. *Water Research* **2018**, *142*, 426–440.

(23) Levermore, J. M.; Smith, T. E.; Kelly, F. J.; Wright, S. L. Detection of Microplastics in Ambient Particulate Matter Using Raman Spectral Imaging and Chemometric Analysis. *Analytical Chemistry* **2020**, *92*, 8732–8740.

(24) Takahashi, T.; Liu, Z.; Thevar, T.; Burns, N.; Mahajan, S.; Lindsay, D.; Watson, J.; Thornton, B. Identification of microplastics in a large water volume by integrated holography and Raman spectroscopy. *Appl. Opt.* **2020**, *59*, 5073–5078.

(25) Kniggendorf, A. K.; Wetzel, C.; Roth, B. Microplastics detection in streaming tap water with raman spectroscopy. *Sensors* **2019**, *19*, 12–14.

(26) Cheng, J.-X.; Xie, X. S. *Coherent Raman scattering microscopy*; CRC press, 2016.

(27) Moura, C. C.; Tare, R. S.; Oreffo, R. O. C.; Mahajan, S. Raman spectroscopy and coherent anti- Stokes Raman scattering imaging: prospective tools for monitoring skeletal cells and skeletal regeneration. *Journal of the Royal Society Interface* **2016**, *13*, 9–11.

(28) Moura, C. C.; Bourdakos, K. N.; tare, R. S.; Oreffo, R. O. C.; Mahajan, S. Live-imaging of Bioengineered Cartilage tissue using Multimodal Non-linear Molecular Imaging. *Scientific Reports* **2019**, *1*, 1–9.

(29) Patel, I. I.; Steuwe, C.; Reichelt, S.; Mahajan, S. Coherent anti-Stokes Raman scattering for label-free biomedical imaging. *Journal of Optics* **2013**, *15*, 094006.

(30) Cavonius, L.; Fink, H.; Kiskis, J.; Albers, E.; Undeland, I.; Enejder, A. Imaging of Lipids in Microalgae with Coherent Anti-Stokes Raman Scattering Microscopy. *Plant physiology* **2015**, *167*, 603–616.

(31) Cole, M.; Lindeque, P.; Fileman, E.; Halsband, C.; Goodhead, R.; Moger, J.; Galloway, T. S. Microplastics ingestion by zooplankton. *Environ. Sci. Technol.* **2013**, *47*, 6646.

(32) Folick, A.; Min, W.; Wang, M. C. Label-free imaging of lipid dynamics using Coherent Anti-stokes Raman Scattering (CARS) and Stimulated Raman Scattering (SRS) microscopy. *Current Opinion in Genetics and Development* **2011**, *21*, 585–590.

(33) Wang, H.-W.; Bao, N.; Le, T. T.; Lu, C.; Cheng, J.-X. Microfluidic CARS cytometry. *Optics express* **2008**, *16*, 5782–5789.

(34) O'Dwyer, K.; Mouras, R.; Mani, A. A.; Rice, D.; Gleeson, M.; Liu, N.; Tofail, S. A. M.; Silien, C. Label-free multimodal coherent anti-Stokes Raman scattering analysis of microparticles in unconstrained microfluidics. *Applied Optics* **2018**, *57*, E32–E36.

(35) Hiramatsu, K.; Ideguchi, T.; Yonamine, Y.; Lee, S. W.; Luo, Y.; Hashimoto, K.; Ito, T.; Hase, M.; Park, J. W.; Kasai, Y.; Sakuma, S.; Hayakawa, T.; Arai, F.; Hoshino, Y.; Goda, K. High-throughput label-free molecular fingerprinting flow cytometry. *Science Advances* **2019**, *5*, 1–9.

(36) Schindelin, J.; Arganda-Carreras, I.; Frise, E.; Kaynig, V.; Longair, M.; Pietzsch, T.; Preibisch, S.; Rueden, C.; Saalfeld, S.; Schmid, B., et al. Fiji: an open-source platform for biological-image analysis. *Nature methods* **2012**, *9*, 676–682.

(37) Pologruto, T. A.; Sabatini, B. L.; Svoboda, K. ScanImage: flexible software for operating laser scanning microscopes. *Biomedical engineering online* **2003**, *2*, 13.

(38) Hendrickson, E.; Minor, E. C.; Schreiner, K. Microplastic Abundance and Composition in Western Lake Superior As Determined via Microscopy, Pyr-GC/MS, and FTIR. *Environmental Science and Technology* **2018**, *52*, 1787–1796.

(39) Willert, C. E.; Gharib, M. Digital particle image velocimetry. *Experiments in fluids* **1991**, *10*, 181–193.

(40) Lindken, R.; Rossi, M.; Große, S.; Westerweel, J. Micro-particle image velocimetry (μPIV): recent developments, applications, and guidelines. *Lab on a Chip* **2009**, *9*, 2551–2567.

(41) Belthangady, C.; Royer, L. A. Applications, promises, and pitfalls of deep learning for fluorescence image reconstruction. *Nature methods* **2019**, *16*, 1215–1225.

(42) Rummel, C. D.; Jahnke, A.; Gorokhova, E.; Kühnel, D.; Schmitt-Jansen, M. Impacts of biofilm formation on the fate and potential effects of microplastic in the aquatic environment. *Environmental Science and Technology Letters* **2017**, *4*, 258–267.

(43) Tu, C.; Chen, T.; Zhou, Q.; Liu, Y.; Wei, J.; Waniek, J. J.; Luo, Y. Biofilm formation and its influences on the properties of microplastics as affected by exposure time and depth in the seawater. *Science of the Total Environment* **2020**, *734*.

(44) Vroom, J. M.; De Grauw, K. J.; Gerritsen, H. C.; Bradshaw, D. J.; Marsh, P. D.; Watson, G. K.; Birmingham, J. J.; Allison, C. Depth penetration and detection of pH gradients in biofilms by two- photon excitation microscopy. *Applied and Environmental Microbiology* **1999**, *65*, 3502–3511.

(45) Gerritsen, H. C.; De Grauw, C. J. Imaging of optically thick specimen using two-photon excitation microscopy. *Microscopy Research and Technique* **1999**, *47*, 206–209.

(46) Sajeesh, P.; Sen, A. K. Particle separation and sorting in microfluidic devices: a review. *Microfluidics and nanofluidics* **2014**, *17*, 1–52.

(47) Lima, A.; Barletta, M.; Costa, M. Seasonal distribution and interactions between plankton and microplastics in a tropical estuary. *Estuarine, Coastal and Shelf Science* **2015**, *165*, 213–225.